The structure of tetrahedral network glass forming systems at intermediate and extended length scales

2007 J. Phys.: Condens. Matter 19 455208

(http://iopscience.iop.org/0953-8984/19/45/455208)

IOP PUBLISHING JOURNAL OF PHYSICS: CONDENSED MATTER

J. Phys.: Condens. Matter **19** (2007) 455208 (16pp) doi:10.1088/0953-8984/19/45/455208

The structure of tetrahedral network glass forming systems at intermediate and extended length scales

Philip S Salmon

Department of Physics, University of Bath, Bath BA2 7AY, UK

Received 24 August 2007
Published 24 October 2007
Online at stacks.iop.org/JPhysCM/19/455208

Abstract

The atomic scale structure of network glass forming systems with the AX_2 stoichiometry is considered and particular attention is paid to the systems $GeSe_2$, $ZnCl_2$ and GeO_2 for which the partial-pair correlation functions have been measured by using the method of isotopic substitution in neutron diffraction. The basic structural motif in all of these systems is the $A(X_{1/2})_4$ tetrahedron, although homopolar bonds are also a significant feature in the case of liquid and glassy $GeSe_2$. The structural motifs link to form a network in which ordering occurs on two different length scales at distances greater than the nearest-neighbour. One of these length scales is associated with an intermediate range and manifests itself by the appearance of a so-called first sharp diffraction peak in the measured diffraction patterns at a scattering vector $k_{\rm FSDP}$ where $k_{\rm FSDP}r_{\rm AX} \simeq 2.5$ and $r_{\rm AX}$ is the nearest-neighbour distance for unlike chemical species. The other is associated with an extended range, which has a periodicity given by $\simeq 2\pi/k_{\rm PP}$, where $k_{\rm PP}$ denotes the scattering vector of the principal peak and $k_{\rm PP}r_{\rm AX} \simeq 4.8$. The nature and interplay between the ordering on the intermediate and extended length scales is characterized and discussed.

(Some figures in this article are in colour only in the electronic version)

1. Introduction

The existence and nature of structure in homogeneous network glass forming systems at distances much greater than the nearest-neighbour has long been a subject of both interest and controversy [1–3]. The object of this paper is to summarize and discuss recent progress on this problem that has been made by applying the method of isotopic substitution in neutron diffraction to measure the full set of partial-pair correlation functions [4]. The focus of attention will be on systems with the AX_2 stoichiometry which are at the heart of many materials of scientific and technological importance [5], where A denotes an electropositive species such as Zn, Ge or Si and X denotes an electronegative species such as Cl, Se or O. It is found that the basic structural motifs, which are usually $A(X_{1/2})_4$ tetrahedra, link to form a network in which two characteristic length scales appear at distances greater than the nearest-neighbour [6]. The first length scale is associated with intermediate range order and manifests itself in the measured

diffraction patterns by a so-called first sharp diffraction peak (FSDP) at a scattering vector $k_{\rm FSDP} \simeq 1$–1.5 Å^{-1} [7–9]. The second length scale is associated with the so-called principal peak at $k_{\rm PP} \simeq 2.0$–2.7 Å^{-1} and appears as oscillations of periodicity given by $\simeq 2\pi/k_{\rm PP}$ which extend to distances well beyond the domain of the FSDP as estimated from the coherence length $2\pi/\Delta k_{\rm FSDP}$ where $\Delta k_{\rm FSDP}$ is the full-width at half-maximum [9]. The nature of the network can be changed substantially by altering the type and connectivity of the basic structural motifs via a change in the atomic constituents or adjustment of the temperature and pressure. The structure can also be changed by, for example, illumination of a chalcogenide glass with light of band-gap energy or below [10].

The neutron diffraction results will be discussed by reference to the so-called Faber–Ziman-pair correlation functions [11], which describe the relative distribution of the atomic species, and also by reference to the so-called Bhatia–Thornton-pair correlation functions [12], which separate the contributions to a measured diffraction pattern from the topological and chemical ordering. Progress has been made possible by the development of improved neutron diffraction instrumentation, particularly the D4C diffractometer at the Institut Laue-Langevin (ILL) in Grenoble [13].

2. Theory

In a neutron diffraction experiment on a liquid or glassy AX_2 system, the coherent scattered intensity can be represented by the total structure factor [14]

$$F(k) = c_{\rm A}^2 b_{\rm A}^2 [S_{\rm AA}(k) - 1] + 2c_{\rm A}c_{\rm X}b_{\rm A}b_{\rm X}[S_{\rm AX}(k) - 1] + c_{\rm X}^2 b_{\rm X}^2 [S_{\rm XX}(k) - 1] \tag{1}$$

where $S_{\alpha\beta}(k)$ represents a Faber–Ziman [11] partial structure factor and c_α, b_α denote the atomic fraction and bound coherent scattering length of chemical species α, respectively. These partial structure factors are related to the partial-pair distribution functions, $g_{\alpha\beta}(r)$, through the Fourier transform relation

$$g_{\alpha\beta}(r) = 1 + \frac{1}{2\pi^2 n_0 r} \int_0^\infty {\rm d}k\, k[S_{\alpha\beta}(k) - 1] \sin(kr), \tag{2}$$

where n_0 is the atomic number density of the system, and the mean number of particles of type β contained in a volume defined by two concentric spheres of radii r_i and r_j, centred on a particle of type α, is given by

$$\bar{n}_\alpha^\beta = 4\pi n_0 c_\beta \int_{r_i}^{r_j} {\rm d}r\, r^2 g_{\alpha\beta}(r). \tag{3}$$

The full set of $S_{\alpha\beta}(k)$ for an AX_2 system can be extracted from the measured diffraction patterns by applying the method of isotopic substitution in neutron diffraction, provided that isotopes with a sufficient neutron scattering length contrast are available [4, 14].

The total structure factor of equation (1) can also be written in terms of the Bhatia–Thornton [12] number–number, concentration–concentration and number–concentration partial structure factors, denoted by $S_{\rm NN}(k)$, $S_{\rm CC}(k)$ and $S_{\rm NC}(k)$ respectively, where

$$\begin{aligned} F(k) = {} & \langle b\rangle^2 [S_{\rm NN}(k) - 1] + c_{\rm A}c_{\rm X}(b_{\rm A} - b_{\rm X})^2 [\{S_{\rm CC}(k)/c_{\rm A}c_{\rm X}\} - 1] \\ & + 2\langle b\rangle (b_{\rm A} - b_{\rm X}) S_{\rm NC}(k) \end{aligned} \tag{4}$$

and $\langle b\rangle = c_{\rm A}b_{\rm A} + c_{\rm X}b_{\rm X}$ is the average scattering length. The relationship between the two sets of partial structure factors is given by

$$\begin{aligned} S_{\rm NN}(k) &= c_{\rm A}^2 S_{\rm AA}(k) + c_{\rm X}^2 S_{\rm XX}(k) + 2c_{\rm A}c_{\rm X}S_{\rm AX}(k) \\ S_{\rm CC}(k) &= c_{\rm A}c_{\rm X}[1 + c_{\rm A}c_{\rm X}(S_{\rm AA}(k) + S_{\rm XX}(k) - 2S_{\rm AX}(k))] \\ S_{\rm NC}(k) &= c_{\rm A}c_{\rm X}[c_{\rm A}(S_{\rm AA}(k) - S_{\rm AX}(k)) - c_{\rm X}(S_{\rm XX}(k) - S_{\rm AX}(k))]. \end{aligned} \tag{5}$$

If $b_A = b_X$ the incident neutrons in a diffraction experiment cannot distinguish between the different scattering nuclei and the measured total structure factor gives $S_{NN}(k)$ directly (see equation (4)). The Fourier transform of $S_{NN}(k)$, the partial-pair distribution function $g_{NN}(r)$, therefore describes the sites of the scattering nuclei and since it cannot distinguish between the chemical species that decorate those sites it gives information on the topological ordering. If $\langle b \rangle = 0$, however, the measured total structure factor gives $S_{CC}(k)$ directly and its Fourier transform, $g_{CC}(r)$, describes the chemical ordering of the A and X atomic species. The partial-pair distribution function $g_{CC}(r)$ will show a positive or negative peak at a given distance when there is a preference for like or unlike neighbours respectively (see equation (7)). The Fourier transform of $S_{NC}(k)$, namely the pair-distribution function $g_{NC}(r)$, describes the correlation between the sites described by $g_{NN}(r)$ and their occupancy by a given chemical species. The relationship between the $g_{\alpha\beta}(r)$ ($\alpha, \beta =$ A, X) and $g_{IJ}(r)$ ($I, J =$ N, C) is given by

$$g_{NN}(r) = c_A^2 g_{AA}(r) + c_X^2 g_{XX}(r) + 2c_A c_X g_{AX}(r) \tag{6}$$

$$g_{CC}(r) = c_A c_X [g_{AA}(r) + g_{XX}(r) - 2g_{AX}(r)] \tag{7}$$

$$g_{NC}(r) = c_A [g_{AA}(r) - g_{AX}(r)] - c_X [g_{XX}(r) - g_{AX}(r)]. \tag{8}$$

3. Results

3.1. Structural signatures for glass formation in liquid AX_2 systems

The measured Bhatia–Thornton partial structure factors for the molten salts $BaCl_2$ [15], $SrCl_2$ [16], $CaCl_2$ [17], $MgCl_2$ [18], $NiCl_2$ [19] and $ZnCl_2$ [20], which have a range of cation to anion radius ratios [21], are shown in figure 1. Zinc dichloride is the only one of these systems which readily forms a glass and the measured $S_{IJ}(k)$ are substantially different to those observed for the other molten AX_2 systems [22]. For example, in the case of $ZnCl_2$ the partial structure factor $S_{NN}(k)$ develops a characteristic 'three-peak' structure in which there is a well-defined FSDP at $k_{FSDP} \simeq 1.03$ Å^{-1}. This feature is the signature of a new level of structural complexity on an intermediate length scale which has a periodicity given by $2\pi/k_{FSDP}$ and a coherence length given by $2\pi/\Delta k_{FSDP}$ [9]. Indeed, all three $S_{IJ}(k)$ for molten $ZnCl_2$ display an FSDP, which occurs at an approximately common value of k_{FSDP}, and all three $S_{IJ}(k)$ also show a well-defined principal peak at a scattering vector k_{PP} which takes a common value of $\simeq 2.1$ Å^{-1}.

By contrast, none of the $S_{IJ}(k)$ for the other liquids shown in figure 1 has a well-defined FSDP and the principal peaks often occur at different values of k. For instance, in the case of $SrCl_2$ the principal peak in $S_{CC}(k)$ occurs at 1.61 Å^{-1} while the principal peak in $S_{NN}(k)$ occurs at 2.31 Å^{-1}. In consequence, it is possible to assign the first and second peaks in the measured total structure factor for this system with the first peaks in $S_{CC}(k)$ and $S_{NN}(k)$ respectively, i.e. the first and second peaks in $F(k)$ can be correctly associated with the chemical and topological ordering [23]. As already discussed, this situation does not hold for $ZnCl_2$ since the principal peaks in all three $S_{IJ}(k)$ occur at a common position.

The measured Bhatia–Thornton $S_{IJ}(k)$ for liquid $GeSe_2$ [24, 25], glassy $GeSe_2$ [26, 27], glassy $ZnCl_2$ [6] and glassy GeO_2 [28, 29] are shown in figure 2. We find that the general features observed in the measured $S_{IJ}(k)$ for liquid $ZnCl_2$ are also seen in the partial structure factors for liquid $GeSe_2$, which likewise forms a glass by bulk quenching methods. Moreover, the generic features in the $S_{IJ}(k)$ for liquid $ZnCl_2$ and $GeSe_2$ carry over to the corresponding glass while there is a concomitant increase in the relative sharpness of the peaks. The corresponding Faber–Ziman partial structure factors, $S_{\alpha\beta}(k)$, are presented in figure 3. They show that the FSDP in all three systems arises predominantly from A–A correlations and that, in

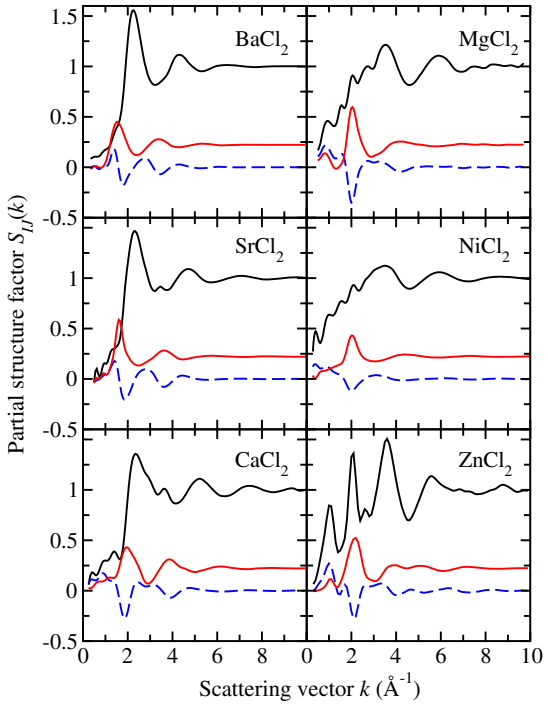

Figure 1. The measured Bhatia–Thornton partial structure factors, $S_{IJ}(k)$, for molten AX_2 systems with varying cation to anion radius ratios (adapted from [22]). For each panel, the upper curve gives $S_{NN}(k)$, the middle (red) curve gives $S_{CC}(k)$ and the lower (blue) broken curve gives $S_{NC}(k)$. On the absolute temperature scale, the ratio of the liquid to melting point temperatures, T/T_{mp}, is 1.051 ($BaCl_2$), 1.045 ($SrCl_2$), 1.045 ($CaCl_2$), 1.017 ($MgCl_2$), 1.013 ($NiCl_2$) and 1.015 ($ZnCl_2$). The cation radii are 1.35 Å (Ba^{2+}), 1.18 Å (Sr^{2+}), 1.00 Å (Ca^{2+}), 0.72 Å (Mg^{2+}), 0.69 Å (Ni^{2+}) and 0.74 Å (Zn^{2+}) and the radius of Cl^- is 1.81 Å [21]. Only the $ZnCl_2$ system readily forms a glass.

Table 1. The mean position of the FSDP, k_{FSDP}, and the principal peak, k_{PP}, for a variety of network glass forming AX_2 systems as scaled by the nearest-neighbour distance for unlike chemical species r_{AX}. The prefixes l and g denote the liquid and glass respectively.

System	r_{AX} (Å)	k_{FSDP} (Å^{-1})	$k_{FSDP}r_{AX}$	k_{PP} (Å^{-1})	$k_{PP}r_{AX}$	Reference
l-$GeSe_2$	2.42(2)	0.98(2)	2.37	2.00(2)	4.84	[25, 27]
g-$GeSe_2$	2.36(2)	1.00(2)	2.36	2.05(3)	4.84	[26, 27]
l-$ZnCl_2$	2.29(2)	1.03(2)	2.36	2.12(3)	4.85	[20]
g-$ZnCl_2$	2.28(1)	1.09(3)	2.49	2.10(1)	4.79	[6]
g-GeO_2	1.73(1)	1.53(2)	2.65	2.66(1)	4.60	[28, 29]
g-SiO_2	1.60(1)	1.50(1)	2.40	2.93(1)	4.69	[28, 29]

the case of glassy GeO_2, there is also a notable contribution from A–X and X–X correlations. Similar observations hold for all the other systems in figure 1 that show a peak in $S_{IJ}(k)$ at $k \simeq 1$ Å^{-1} [22]. The development of an intermediate length scale is therefore related to the relative distribution of structural motifs associated with the A atoms. The mean FSDP and principal peak positions for several network glass forming AX_2 systems are shown in table 1. When scaled by r_{AX}, the nearest-neighbour distance for unlike chemical species, it is found that $k_{FSDP}r_{AX} \simeq 2.5$ (see [30] for further discussion) and $k_{PP}r_{AX} \simeq 4.8$.

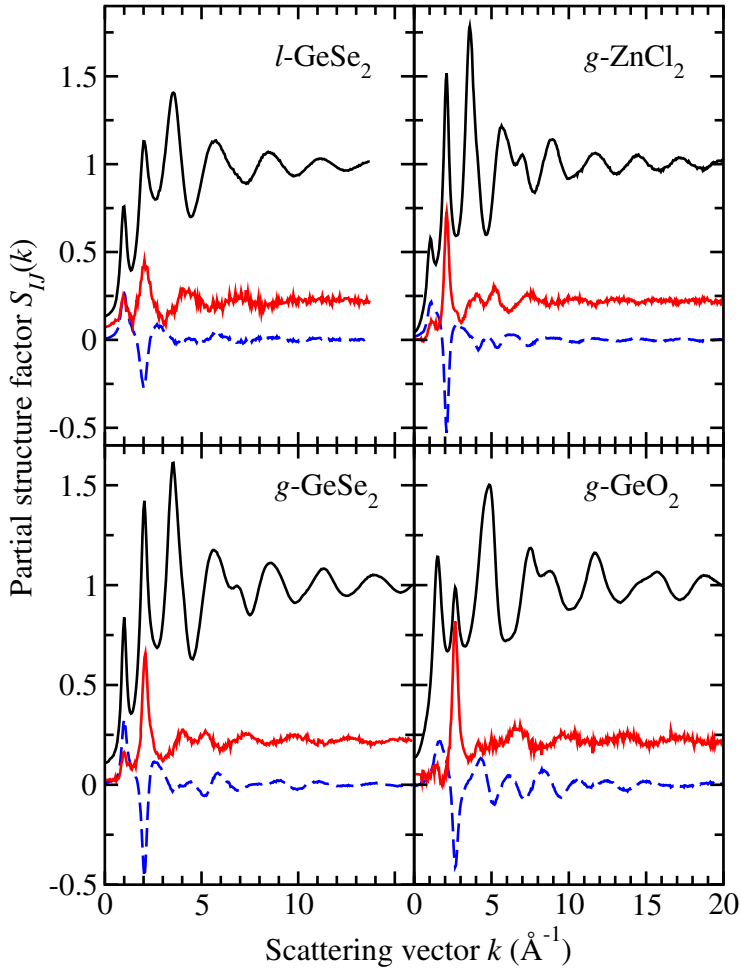

Figure 2. The measured Bhatia–Thornton partial structure factors, $S_{IJ}(k)$, for liquid $GeSe_2$ [25], glassy $GeSe_2$ [26, 27], glassy $ZnCl_2$ [6] and glassy GeO_2 [28, 29]. For each panel, the upper curve gives $S_{NN}(k)$, the middle (red) curve gives $S_{CC}(k)$ and the lower (blue) broken curve gives $S_{NC}(k)$. The statistical uncertainties are represented by the scatter in the data points. On the absolute temperature scale, the ratio of the liquid to melting point temperatures, T/T_{mp}, is 1.041 for $GeSe_2$. The diffraction measurements for the glasses were all made at ≈25 °C.

3.2. Structure of network glass forming AX_2 systems

The measured partial-pair distribution functions $g_{\alpha\beta}(r)$ for liquid and glassy $GeSe_2$, glassy $ZnCl_2$ and glassy GeO_2 are illustrated in figure 4 and several of the parameters describing the local structure are listed in table 2. The atomic number density for these systems is 0.0311(2) Å^{-3} [24], 0.0334(1) Å^{-3} [26], 0.0359(1) Å^{-3} [6] and 0.0629(3) Å^{-3} [28] respectively. In table 2, the A–$\hat{\text{X}}$–A bond angle, θ_{AXA}, was calculated from the quoted A–X and A–A distances, r_{AX} and r_{AA}, by using $\cos(\theta_{AXA}) = 1 - r_{AA}^2/2r_{AX}^2$. For each system, the coordination number for unlike chemical species $\bar{n}_A^X$ and the distance ratio r_{AA}/r_{AX} are consistent with the appearance of $A(X_{1/2})_4$ tetrahedra as the predominant structural motifs. The distance ratio r_{AA}/r_{AX} for perfect tetrahedra is $\sqrt{8/3} = 1.633$ which suggests that the

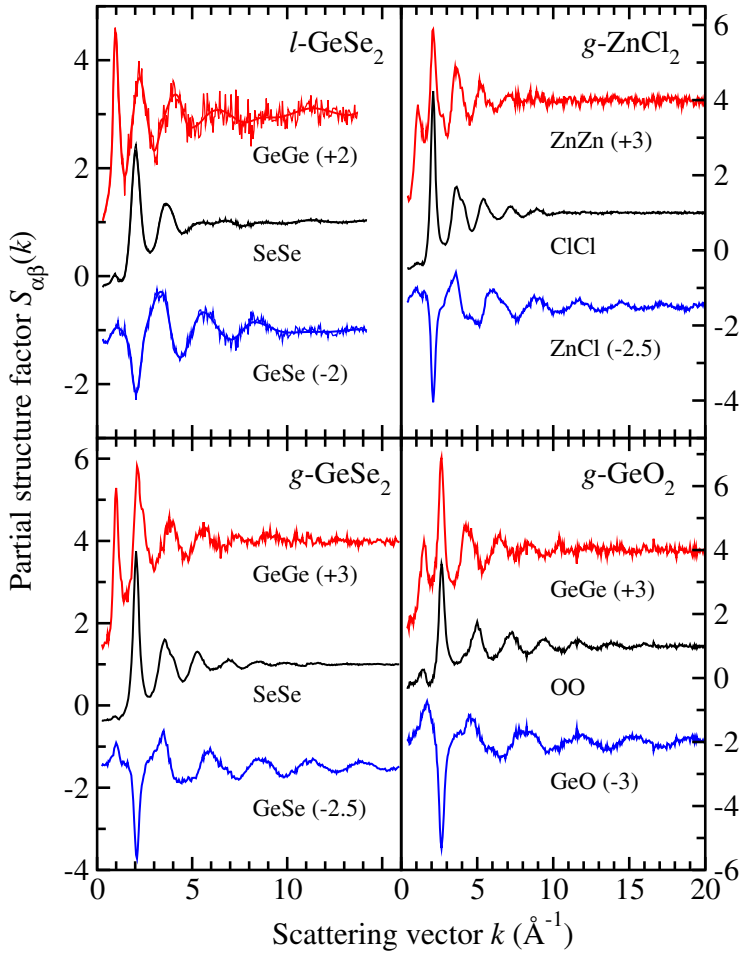

Figure 3. The measured Faber–Ziman partial structure factors, $S_{\alpha\beta}(k)$, for liquid $GeSe_2$ [25], glassy $GeSe_2$ [26, 27], glassy $ZnCl_2$ [6] and glassy GeO_2 [28, 29]. For each panel, the upper (red) curve gives $S_{AA}(k)$, the middle (black) curve gives $S_{XX}(k)$, and the lower (blue) curve gives $S_{AX}(k)$. The statistical uncertainties are represented by the scatter in the data points.

tetrahedra in liquid $GeSe_2$ are relatively distorted. The first peak in $g_{AX}(r)$ for glassy GeO_2 is very sharp by comparison with the other materials and coincides with higher vibrational frequencies [31–33]. It yields a coordination number $\bar{n}^{O}_{Ge}$ that is systematically less than four owing to the finite k-space resolution function of the diffractometer for which a correction was not made [34, 35].

In the case of $GeSe_2$, homopolar Ge–Ge and Se–Se bonds are observed at 2.33(3) and 2.30(2) Å for the liquid and at 2.42(2) and 2.32(2) Å for the glass and correspond to coordination numbers of $\bar{n}^{Ge}_{Ge} = 0.25(10)$, $\bar{n}^{Se}_{Se} = 0.23(5)$ and $\bar{n}^{Ge}_{Ge} = 0.25(5)$, $\bar{n}^{Se}_{Se} = 0.20(5)$ respectively [27]. The nearest-neighbour coordination number for unlike chemical species, $\bar{n}^{Se}_{Ge}$, is 3.5(2) for the liquid and 3.7(1) for the glass (see table 2). Hence the overall Ge and Se coordination numbers $\bar{n}_{Ge} = \bar{n}^{Ge}_{Ge} + \bar{n}^{Se}_{Ge}$ and $\bar{n}_{Se} = \bar{n}^{Se}_{Se} + \bar{n}^{Ge}_{Se}$ are 3.8(2) and 2.0(1) for the liquid together with 4.0(1) and 2.05(7) for the glass respectively, i.e. Ge and Se are, within the experimental error, four-fold and two-fold coordinated and therefore have a full outer shell of eight electrons. For the glass, it is also possible to discern a peak at 3.02(2) Å in $g_{GeGe}(r)$

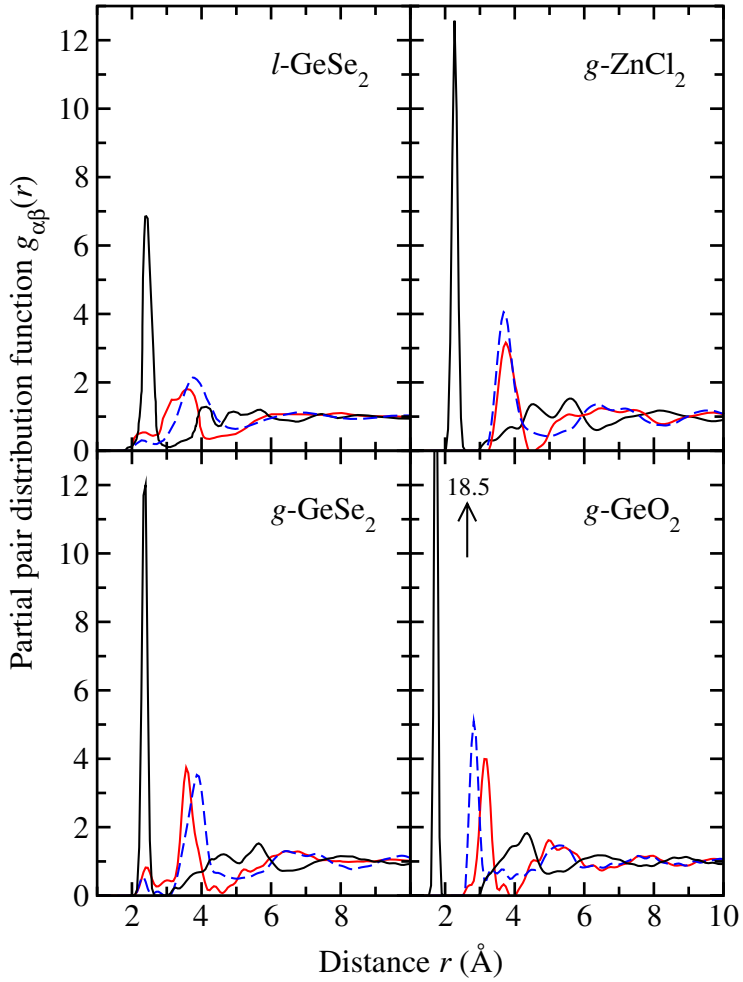

Figure 4. The measured partial-pair distribution functions, $g_{\alpha\beta}(r)$, for liquid $GeSe_2$ [25], glassy $GeSe_2$ [26, 27], glassy $ZnCl_2$ [6] and glassy GeO_2 [28, 29]. For each panel, the dark curve gives $g_{AX}(r)$, the light (red) curve gives $g_{AA}(r)$ and the broken (blue) curve gives $g_{XX}(r)$. In the case of the glassy systems, the effect in real space of truncating the diffraction pattern at a finite maximum k value before Fourier transformation was taken into account by using the procedure described in [27]. The unphysical low-r oscillations have been suppressed for clarity of presentation.

(see figure 4), which is identified with the Ge–Ge distance within an edge-sharing tetrahedral motif for which the Ge–$\hat{\text{S}}$e–Ge bond angle is 80(1)° (the mean Ge–$\hat{\text{S}}$e–Ge bond angle for other tetrahedral configurations is 98(1)°—see table 2.) The accompanying coordination number $\bar{n}^{\text{Ge}}_{\text{Ge}} = 0.34(5)$ is consistent with a ratio for the number of Ge in edge-sharing tetrahedra to the total number of Ge in the system of 34(5)%, in agreement with several other estimates [27]. Liquid and glassy $GeSe_2$ also contain corner-sharing $Ge(Se_{1/2})_4$ tetrahedra in accordance with the structure of the high-temperature phase of crystalline $GeSe_2$ which has equal numbers of edge- and corner-sharing tetrahedral motifs [36]. The ratio for the number of Ge in edge-sharing tetrahedra to the number of Ge in corner-sharing tetrahedra, obtained from the neutron diffraction experiments, is roughly comparable for the liquid [25] and is 83(16)% for the glass [27].

Table 2. Parameters obtained from the first main peaks in the measured $g_{\alpha\beta}(r)$ for liquid and glassy $GeSe_2$, glassy $ZnCl_2$ and glassy GeO_2. The coordination numbers were calculated by using a cut-off value equal to the first minimum after a peak in $g_{\alpha\beta}(r)$. For liquid and glassy $GeSe_2$, peaks also occur in $g_{GeGe}(r)$ and $g_{SeSe}(r)$ at smaller values of r and correspond to the appearance of homopolar bonds and edge-sharing tetrahedra. For ideal tetrahedral units $r_{XX}/r_{AX} = \sqrt{8/3} = 1.633$.

System	$g_{\alpha\beta}(r)$	$r_{\alpha\beta}$ (Å)	$\bar{n}_\alpha^\beta$	Range (Å)	r_{XX}/r_{AX}	A–$\hat{X}$–A (deg)	η'_X	Reference
l-$GeSe_2$	GeSe	2.42(2)	3.5(2)	1.8–3.1	1.550(15)	96(1)	0.670(17)	[25, 27]
	GeGe	3.59(2)	2.9(3)	2.6–4.2				
	SeSe	3.75(2)	9.6(3)	2.7–4.8				
g-$GeSe_2$	GeSe	2.36(2)	3.7(1)	2.09–2.61	1.648(16)	80(1)[a], 98(1)	0.667(17)	[26, 27]
	GeGe	3.57(2)	3.2(3)	3.19–4.23				
	SeSe	3.89(2)	9.3(2)	3.09–4.39				
g-$ZnCl_2$	ZnCl	2.28(1)	3.9(1)	1.90–2.70	1.623(8)	111(1)	0.647(9)	[6]
	ZnZn	3.75(1)	4.0(1)	3.31–4.42				
	ClCl	3.70(1)	12.1(2)	3.19–4.97				
g-GeO_2	GeO	1.73(1)	3.8(1)	1.53–1.96	1.636(11)	132(2)	0.495(9)	[28, 29]
	GeGe	3.16(1)	4.1(2)	2.58–3.56				
	OO	2.83(1)	6.7(1)	2.58–3.13				

[a] The Ge–$\hat{S}$e–Ge angle for edge-sharing tetrahedra as calculated by using the measured value of $r_{GeGe} = 3.02(2)$ Å for this structural conformation.

By comparison to $GeSe_2$, the structure of $ZnCl_2$ and GeO_2 is based predominantly on corner-sharing $A(X_{1/2})_4$ tetrahedra, i.e. the diffraction experiments do not show evidence for homopolar bonds or for edge-sharing conformations (the maximum nearest neighbour A–A distance for regular edge-sharing tetrahedra is $r_{AA} = 2\cos(\theta_{XAX}/2)r_{AX} = 1.155r_{AX}$ where $\theta_{XAX} = \cos^{-1}(-1/3) = 109.47°$ is the tetrahedral angle). In general, the packing fraction of spherical X atoms of radius r_X in an AX_2 system is $\eta'_X = (8/9)n_0\pi r_X^3$ and for a perfect tetrahedron of four spherical touching X atoms, $r_{XX}/r_{AX} = \sqrt{8/3}$ where $r_{XX} = 2r_X$. Hence the packing fraction of X atoms in tetrahedral units, expressed as a function of r_{AX} and the atomic number density n_0, is $\eta'_X = 16\sqrt{2}\pi n_0 r_{AX}^3/27\sqrt{3} = 1.520 n_0 r_{AX}^3$ [37]. The values of η'_X listed in table 2 show the extent to which the network opens up as the inter-tetrahedral bond angle A–$\hat{X}$–A increases on going from glassy $ZnCl_2$ to GeO_2. It is notable that the anion packing fraction for glassy $ZnCl_2$ is close to the value of $\simeq$0.64 found for a dense random packing of hard spheres [38]. In the case of $GeSe_2$, the assumption of spherical X atoms in regular tetrahedral units leads to $\eta'_X = 0.667(17)$ for the glass and $\eta'_X = 0.6836$ for the high-temperature crystalline phase [37], which suggests a softening of the spheres and deformation of the tetrahedra. Nevertheless, it is possible to calculate a reduced packing fraction for hard sphere X atoms in glassy $GeSe_2$ by considering the homopolar bonding motifs. For example, if only dimers are formed it follows that the ratio for the maximum fraction of Se involved in homopolar bonds to the total number of Se atoms in the system is given by 20(5)% [27] and the measured distance for Se–Se homopolar bonds gives a radius $r_{Se} = 1.16$ Å. The packing fraction of Se atoms, assuming 20% Se in dimers and 80% Se in $Ge(Se_{1/2})_4$ tetrahedra, is then given by $\eta'_X = 0.2(8n_0\pi r_{Se}^3/9) + 0.8(1.520 n_0 r_{GeSe}^3) = 0.56$ where $r_{GeSe} = 2.36$ Å.

4. Discussion

4.1. Intermediate range order and the first sharp diffraction peak

As already discussed, the FSDP is regarded as a signature of ordering on an intermediate length scale and, as befits the appearance of a sharp peak in reciprocal space, the periodicity of this

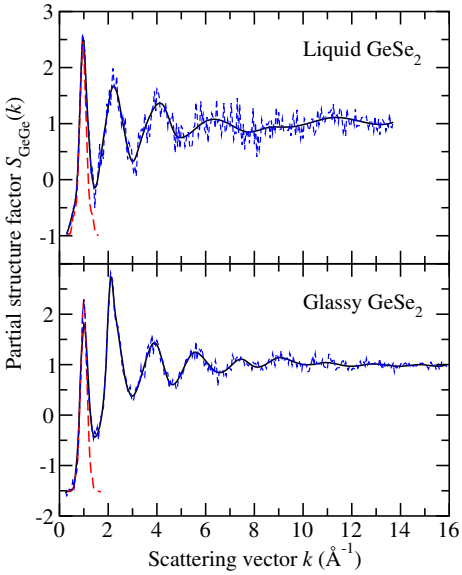

Figure 5. The measured partial structure factor $S_{\mathrm{GeGe}}(k)$ for liquid $GeSe_2$ at 784 °C [25] and glassy $GeSe_2$ at 26 °C [26, 27]. For each panel, the broken (blue) curve joins the data points, the solid (black) curve gives a spline fit to the data, and the broken (red) curve gives the FSDP as obtained by reflecting the low-k part of the first peak about its maximum at k_{FSDP}.

ordering is given by $2\pi/k_{\mathrm{FSDP}}$ and the coherence length is given by $2\pi/\Delta k_{\mathrm{FSDP}}$ where Δk_{FSDP} is the full-width at half-maximum [9]. It is, however, very difficult to discern this ordering in the corresponding partial-pair distribution functions. As an illustration, we therefore consider the case of liquid and glassy $GeSe_2$ where the FSDP in $S_{\mathrm{GeGe}}(k)$ is a particularly prominent feature (see figure 3). The contribution of the FSDP to the ordering in r-space is estimated by reflecting the low-k portion of the first peak about k_{FSDP} in order to separate it from the other features in $S_{\mathrm{GeGe}}(k)$ (see figure 5). The FSDP thus obtained is then Fourier transformed to compare with the full $g_{\mathrm{GeGe}}(r)$ function as shown in figure 6. Finally, the Fourier transform of the FSDP is subtracted from $g_{\mathrm{GeGe}}(r)$ to give $\tilde{g}_{\mathrm{GeGe}}(r)$ and the result is also presented in figure 6 in terms of the function $r\tilde{g}_{\mathrm{GeGe}}(r)$ which emphasizes the nature of the ordering at large r-values [39]. In the case of liquid $GeSe_2$, two curves are shown for $g_{\mathrm{GeGe}}(r)$, corresponding to an analysis of the data where Ge–Ge homopolar bonds were either allowed or excluded (see [25] and the discussion in [40, 41]). The results show that the Fourier transform of the FSDP in $S_{\mathrm{GeGe}}(k)$ does account for discernable real space features in $g_{\mathrm{GeGe}}(r)$. In the case of the glass, when the underlying modulation due to the FSDP is subtracted the resultant function $r\tilde{g}_{\mathrm{GeGe}}(r)$ shows oscillations about zero which persist to large distances. The character of this extended range ordering in network glass forming systems, which is *not* associated with the FSDP, will now be considered in greater detail.

4.2. Ordering on an extended length scale in AX_2 glasses

For several reasons the extended range ordering in AX_2 glasses is most conveniently considered in terms of the Bhatia–Thornton partial-pair distribution functions. Firstly, the Bhatia–Thornton partial structure factors for the measured systems are usually better conditioned than the corresponding Faber–Ziman partial structure factors and are therefore less prone to systematic

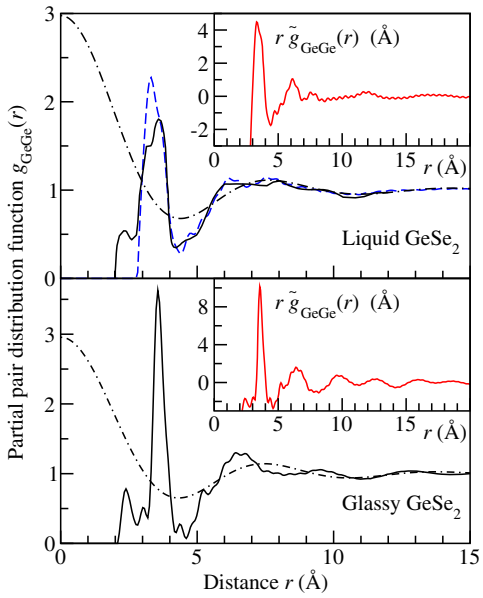

Figure 6. The measured partial-pair distribution function $g_{GeGe}(r)$ for (a) liquid and (b) glassy $GeSe_2$ as obtained from the partial structure factors shown in figure 5. Two curves are given for the liquid and correspond to an analysis of the data in which homopolar bonds were either allowed (full curve) or excluded (broken (blue) curve)—see the text for further details. Each $g_{GeGe}(r)$ function is compared with the Fourier transform (chained curve) of the FSDP in $S_{GeGe}(k)$ which is shown by the broken (red) curve in figure 5. The insets show the function $r\tilde{g}_{GeGe}(r)$ which illustrates the effect of subtracting the Fourier transform of the FSDP from the measured Ge–Ge partial-pair distribution function.

error [34]. Secondly, the Bhatia–Thornton formalism focuses on the number density and concentration fluctuations and thereby allows for a separation of the contributions to the structure from the topological and chemical ordering [22]. Thirdly, the low-k limits of the partial structure factors and the moments of the partial-pair correlation functions can be readily linked to the thermodynamic and other properties of a system [12, 34, 42]. Lastly, an analysis of the large-r behaviour of the Bhatia–Thornton-pair correlation functions for simple model pair potentials leads to simple analytical expressions for their ultimate decay [34].

Consider, for example, a rigid-ion potential which represents one of the simplest simulation models for ionic systems [43–45]. Let the chemical species A and X have positive and negative charges of $Z_A e$ and $Z_X e$ respectively, where e is the elementary charge, and let the interaction between any two particles labelled by i and j separated by a distance r be represented by a pair potential which contains a short-ranged repulsive term $\phi_{ij}^{sr}(r)$, a Coulomb term $\phi_{ij}^{Coul}(r) \propto r^{-1}$, and a dispersion term $\phi_{ij}^{disp}(r) \propto r^{-6}$ such that

$$\phi_{ij}(r) = \phi_{ij}^{sr}(r) + \frac{Z_i Z_j e^2}{\epsilon\, r} - \frac{A_{ij}}{r^6} \tag{9}$$

where $\epsilon \equiv 4\pi\varepsilon_r\varepsilon_0$, ε_r is the dimensionless relative dielectric constant of the medium in which the ions are immersed and ε_0 is the vacuum permittivity. The dispersion term results from induced dipole–induced dipole interactions and A_{ij} is a parameter ($\geqslant 0$) which depends on the polarizability of the ions [46].

For the rigid-ion model, a simple power-law dependence for the ultimate decay of the pair correlation functions is expected where $rh_{NN}(r) \to r^{-5}$, $rh_{NC}(r) \to r^{-7}$, $rh_{CC}(r) \to r^{-9}$

Table 3. Parameters obtained by fitting the measured Bhatia–Thornton-pair correlation functions $rh_{IJ}(r)$ for glassy $GeSe_2$, $ZnCl_2$ and GeO_2 by using equations (10)–(12).

System	IJ	a_0 (Å^{-1})	a_0^a (Å^{-1})	a_1 (Å^{-1})	k_{PP} (Å^{-1})	A_{IJ}^b (Å)	θ_{IJ} (rad)	R^2	Range (Å)
g-$GeSe_2$	NN	0.24(2)	0.29(5)	2.10(2)	2.04(1)	3(1)	−2.6(4)	0.95	15.6–21.0
	CC	0.180(4)	0.185(9)	2.093(4)	2.09(1)	4.0(2)	−1.68(4)	0.98	7.6–19.4
	NC	0.158(9)	0.21(3)	2.104(8)	2.05(1)	3.1(4)	−5.3(1)	0.96	10.8–19.8
g-$ZnCl_2$	NN	0.17(1)	0.20(2)	2.11(1)	2.09(1)	1.1(2)	−1.8(2)	0.91	15.2–25.6
	CC	0.225(5)	0.204(7)	2.133(5)	2.10(1)	8.5(4)	−1.89(5)	0.97	7.7–26.9
	NC	0.183(4)	0.184(7)	2.119(3)	2.10(1)	5.4(3)	1.34(5)	0.98	10.5–25.5
g-GeO_2	NN	0.33(3)	0.26(4)	2.78(3)	2.67(1)	2.1(8)	2.8(4)	0.86	12.3–19.9
	CC	0.24(1)	0.25(2)	2.62(1)	2.65(1)	6.3(5)	−1.26(7)	0.94	4.7–15.4
	NC	0.250(5)	0.26(1)	2.654(5)	2.66(1)	4.7(2)	1.66(5)	0.99	7.1–16.6

[a] From a straight line fit to the maxima in $\ln|rh_{IJ}(r)|$ versus r.
[b] $A_{NN} \equiv 2|\mathcal{A}_{NN}|$, $A_{CC} \equiv 2c_A c_X|\mathcal{A}_{CC}|$ and $A_{NC} \equiv 2|\mathcal{A}_{NC}|$.

and $h_{NN}(r) \equiv g_{NN}(r) - 1$, $h_{NC}(r) \equiv g_{NC}(r)$, $h_{CC}(r) \equiv g_{CC}(r)$ [34, 47]. However, if the dispersion terms are absent in equation (9) then a pole analysis of the k-space solutions to the Ornstein–Zernike equations, following the method of Evans and co-workers [48, 49], leads to the following expressions for the asymptotic decay of the pair correlation functions when the system density is high [34]:-

$$rh_{NN}(r) \to 2|\mathcal{A}_{NN}| \exp(-a_0 r)\cos(a_1 r - \theta_{NN}) \tag{10}$$

$$rh_{CC}(r) \to 2c_A c_X|\mathcal{A}_{CC}| \exp(-a_0 r)\cos(a_1 r - \theta_{CC}) \tag{11}$$

$$rh_{NC}(r) \to 2|\mathcal{A}_{NC}| \exp(-a_0 r)\cos(a_1 r - \theta_{NC}). \tag{12}$$

In this case, the correlations have an exponentially damped oscillatory decay with a common decay length given by a_0^{-1} and a common wavelength for the oscillations given by $2\pi/a_1$. The $\mathcal{A}_{IJ}$ are complex numbers with amplitudes related by $|\mathcal{A}_{NN}||\mathcal{A}_{CC}| = |\mathcal{A}_{NC}|^2$ and phases related by $\theta_{NN} + \theta_{CC} = 2\theta_{NC}$. Equations (10)–(12) also hold for a hard sphere system when both the Coulomb and dispersion terms are absent in equation (9).

For the rigid-ion model, a power-law decay might be difficult to observe owing to the relative weakness of the dispersion forces. However, the presence of these forces means that equations (10)–(12) will not necessarily hold since they were derived for the case when dispersion forces are absent. Furthermore, the presence of three- or higher-body interactions for glass forming AX_2 systems also provides complications since the theory is based on pair potentials. However, provided the large-r interactions can be described by effective pair potentials that lead to simple poles [34], it is feasible that the theory which leads to equations (10)–(12) will remain valid. Notwithstanding, these equations provide a benchmark for analysing the large r-dependence of the Bhatia–Thornton-pair distribution functions and for understanding the origin of ordering on an extended range in more complicated systems that involve three-body potentials.

The ordering on an extended length scale in AX_2 network glasses is conveniently illustrated by reference to the results obtained for glassy $ZnCl_2$ [6], especially as this system is expected to fall within the framework of an ionic interaction model provided that ion polarization effects are taken into account [44]. The $h_{IJ}(r)$ functions for this material were obtained by spline fitting and Fourier transforming the $S_{IJ}(k)$ after (i) the low-k data points ($k \leqslant 0.40$ Å^{-1}) were extrapolated to $k = 0$ by plotting either $[S_{NN}(k)-1]$, $[S_{CC}(k)/c_{Zn}c_{Cl}-1]$ or $S_{NC}(k)/c_{Zn}c_{Cl}$ versus k^2 and fitting a straight line at small-k [42] and (ii) a Lorch modification function was applied [50]. The resultant functions, plotted as $\ln|rh_{IJ}(r)|$ versus r in figure 7,

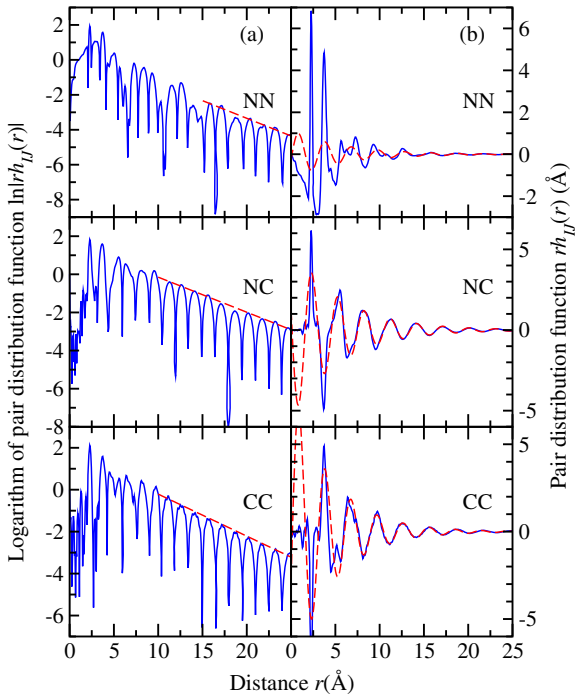

Figure 7. Decay of the Bhatia–Thornton partial-pair distribution functions for glassy $ZnCl_2$ as shown by plotting $\ln|rh_{IJ}(r)|$ versus r (solid (blue) curves) in column (a) and $rh_{IJ}(r)$ versus r (solid (blue) curves) in column (b). For column (a), the inverse decay length a_0 was obtained from the fitted straight lines given by the broken (red) curves and it takes a value of 0.20(2) $Å^{-1}$ (fit range 15.8–24.8 Å, $R^2 = 0.97$), 0.184(7) $Å^{-1}$ (fit range 11.3–24.7 Å, $R^2 = 0.99$) and 0.204(7) $Å^{-1}$ (fit range 8.1–26.3 Å, $R^2 = 0.99$) for the N–N, N–C and C–C functions respectively. For column (b), the broken (red) curves show the fits to the $rh_{IJ}(r)$ functions at large r-values (see [34] for further details).

show that the N–N correlations have a greater complexity than the N–C and C–C correlations and decay more rapidly at smaller-r values. All of the functions show ordering at large-r values which persists to distances far exceeding the coherence length $2\pi/\Delta k_{\mathrm{FSDP}} \simeq 12.6$ Å estimated from the width of the FSDP in $S_{\mathrm{NN}}(k)$. The inverse decay length a_0 was estimated by fitting the repeated maxima at large-r in figure 7, which are least sensitive to the details of any smoothing procedure, to the straight line

$$\ln|rh_{IJ}(r)| = -a_0 r + \text{constant}. \tag{13}$$

The $rh_{IJ}(r)$ functions were also fitted by using equations (10)–(12) (see figure 7) and the fitted parameters, the range used for the fits and the R^2 goodness-of-fit parameter are summarized in table 3. The a_0 values thus deduced represent upper limits owing to the k-space resolution function of the diffractometer [34]. The results show that the extended range oscillations for glassy $ZnCl_2$ decay exponentially with a common inverse decay length $a_0 \simeq 0.19$ $Å^{-1}$ and a periodicity that is determined not by the position of the FSDP but by the position of the principal peak i.e. the wavelength of the oscillations $2\pi/a_1 \simeq 2\pi/k_{\mathrm{PP}}$. Indeed, equations (11) and (12) provide a robust account of the measured $rh_{\mathrm{CC}}(r)$ and $rh_{\mathrm{NC}}(r)$ functions to distances as short as $\simeq 5$ Å. The relationship between the amplitudes predicted by the simple theory does not, however, appear to hold. Similar conclusions are drawn from an analysis of the measured

$rh_{IJ}(r)$ functions for glassy $GeSe_2$ and GeO_2, as indicated by the parameters summarized in table 3 [29, 34].

It is notable that exponentially damped oscillatory $rh_{IJ}(r)$ functions for network glasses will not be reproduced by models based on crystalline systems since the ordering in $rh_{IJ}(r)$ will persist to arbitrarily large distances [51], even when a large positional disorder is applied to the atomic coordinates [52, 53].

4.3. Ordering on intermediate versus extended length scales with increasing glass fragility

It is found that the measured Bhatia–Thornton partial structure factors, $S_{IJ}(k)$, for glassy $GeSe_2$ are comparable to the corresponding $S_{IJ}(k)$ for glassy $ZnCl_2$ when these functions are plotted in terms of the scaled scattering vector kr_{AX} (see figure 2 of [6]). A similar observation holds when the N–C and C–C partial structure factors for these systems are compared to those measured for glassy GeO_2, although the N–N partial structure factor for glassy GeO_2 is markedly different in having a much larger FSDP and smaller principal peak (see figure 1 of [28]). It is therefore plausible that there is a correlation between the relative importance of the ordering on the intermediate and extended length scales (as manifested by the features in the N–N partial structure factor) and the packing of the basic structural motifs (as represented by parameters such as the A–$\hat{X}$–A bond angle and anion packing fraction η'_X which are given in table 2). On the fragility scale, GeO_2 is like silica (SiO_2) in being an archetypal 'strong' glass forming material, a taxonomy which stems originally from the temperature dependence of the liquid viscosity [54]. By comparison, $GeSe_2$ and $ZnCl_2$ are more intermediate in character between the 'strong' and 'fragile' extremes [54, 55]. Thus it is the relative importance of the FSDP and principal peak in $S_{NN}(k)$ that most readily enables a distinction to be made between the diffraction patterns measured for the 'strong' glass former GeO_2 and the more 'intermediate' glass formers $GeSe_2$ and $ZnCl_2$.

The generality of this observation can be tested by investigating the density dependence of the structure of liquid and glassy $GeSe_2$ by using x-ray and neutron diffraction methods since the fragility of a liquid or glass is expected to increase with density [56–58] and the measured total structure factor for $GeSe_2$ usually gives an excellent representation of $S_{NN}(k)$ [39, 59]. This follows because in a neutron diffraction experiment on $GeSe_2$ containing elements of natural isotopic abundance $b_{Ge} \approx b_{Se}$ in equation (4) so that $F(k) \simeq \langle b \rangle^2 [S_{NN}(k) - 1]$. In a conventional x-ray diffraction experiment, $S_{NN}(k)$ is again obtained directly from the measured diffraction pattern since the atomic form factors of Ge and Se, which replace the coherent neutron scattering lengths for Ge and Se in equation (4), are also comparable. When the pressure on glassy $GeSe_2$ is increased from ambient to 9.3 GPa, it is found that the FSDP in $S_{NN}(k)$ vanishes and the principal peak gains in intensity [60]. Similar behaviour for $S_{NN}(k)$ is observed for the liquid phase of $GeSe_2$ as the density is increased at constant temperature by applying a pressure between 0.5 and 4.1 GPa at 847 °C [61]. When the temperature of liquid $GeSe_2$ is increased at much lower pressures from 742–1100 °C, the density also *increases* as the network collapses [62] and the FSDP in $S_{NN}(k)$ diminishes in intensity relative to the principal peak [63].

4.4. Origin of the ordering on an extended length scale

As for the FSDP, the principal peak also appears as a sharp feature in the measured $S_{IJ}(k)$ for the AX_2 systems shown in figure 2. It is therefore expected to give rise to oscillations in real space with a periodicity given by $2\pi/k_{PP}$ and a coherence length given by $2\pi/\Delta k_{PP}$ where Δk_{PP} is the full-width at half-maximum. For example, a principal peak with a Lorentzian profile will give rise to exponentially damped oscillations in real space with an inverse decay length

given by $\Delta k_{\rm PP}/2$ [9]. In the case of glassy $ZnCl_2$, $\Delta k_{\rm FSDP} \simeq 0.50$ Å^{-1} and $\Delta k_{\rm PP} \simeq 0.38$ Å^{-1}, which give inverse decay lengths for the intermediate and extended range oscillations of $\simeq$0.25 and 0.19 Å^{-1} respectively. These values are comparable to the inverse decay lengths obtained from the data given in figure 7; a fit using equation (13) to the N–N correlations in the intermediate range ($\approx$5–9 Å^{-1}) gives an inverse decay length of $\simeq$0.26 Å^{-1} while a fit to the extended range oscillations gives $a_0 = 0.20(2)$ Å^{-1} (see table 3). This accounts for an initial decay of the correlations in $\ln|rh_{\rm NN}(r)|$ (see figure 7) that is more rapid than at the largest r values. The estimated widths of the principal peaks in $S_{\rm CC}(k)$ and $S_{\rm NC}(k)$ (measured relative to a peak height defined by drawing a baseline between adjacent minima) give inverse decay lengths of 0.19 and 0.16 Å^{-1}, respectively, that are also in fair accord with the a_0 values quoted in table 3. Furthermore, the wavelength $2\pi/k_{\rm PP}$ of the extended range oscillations is comparable to the size of a tetrahedral $A(X_{1/2})_4$ motif e.g. for the AX_2 systems listed in table 1 we find that $2\pi/k_{\rm PP} \approx 4r_{\rm AX}/3$, which is the base to apex distance in a regular tetrahedron, whence $k_{\rm PP}r_{\rm AX} \approx 3\pi/2 \approx 4.7$. Hence, the extended range oscillations observed for network glass forming AX_2 systems arise from a local ordering phenomenon which has a *long* coherence length.

For dense hard sphere liquids, extended range oscillations occur in $rh_{\rm NN}(r)$ and have a periodicity that is dependent on the hard sphere diameter [65, 66]. For molten salts, extended range oscillations occur in $rh_{\rm CC}(r)$ and are attributed to a competition between packing effects and screening which leads to charge ordering of the ions and to the appearance of a relatively sharp principal peak in $S_{\rm CC}(k)$ [67]. As shown in figure 1, however, the existence of charge ordering alone is insufficient to produce the type of structure that is observed in network glass forming AX_2 systems. For example, the principal peaks in the $S_{IJ}(k)$ do not generally occur at a common position and a mere packing of charge neutral units does not lead inextricably to a well-defined FSDP. Instead, the measured behaviour of the Bhatia–Thornton-pair distribution functions and their moments (see figure 2 of [42] and section 2.6 of [34]) shows that the ordering on an extended range must result from two interdependent effects.

Firstly, the oscillations in $rh_{\rm CC}(r)$ show a preference for chemical ordering, i.e. a linkage of the basic structural motifs that gives alternating A–X–A–X configurations. Secondly, this chemical ordering is coupled with the topological ordering since $rh_{\rm NC}(r)$ also shows marked oscillations, having a common wavelength of oscillation $\simeq 2\pi/k_{\rm PP}$, which extend to large distances (see figure 7). The basic structural motifs therefore pack to give number density fluctuations represented by $rh_{\rm NN}(r)$ that occur on the *same* length scale as the concentration fluctuations represented by $rh_{\rm CC}(r)$. As indicated by figure 6 (b), the arrangements thus formed also produce a modulation of the pair-distribution functions on an *intermediate* scale as manifested by the appearance of an FSDP in $S_{\rm NN}(k)$. The discussion of section 4.3 shows that the FSDP increases in importance relative to the principal peak with increasing openness of the network structure which is characterized by parameters such as the A–$\hat{\rm X}$–A bond angle and anion packing fraction $\eta'_{\rm X}$. As an additional example, the diffraction pattern for glassy SiO_2 features a more prominent FSDP and weaker principal peak than for glassy GeO_2 (see figure 4 in [28]) and corresponds to an A–$\hat{\rm X}$–A bond angle that is larger at 148° [64] and a packing fraction of oxygen atoms that is smaller at $\eta'_{\rm X} = 0.414(8)$ [29].

Finally, so-called polyamorphic phase transitions are associated with an abrupt change in the structure of a liquid or glass from strong to fragile with increasing density [56–58] and tetrahedrally bonded systems remain the most promising candidates for studying this phenomenon experimentally [68, 69]. Furthermore, two or more competing length scales are built into simple model pair-potentials that are used in calculations to examine the feasibility of liquid–liquid phase transitions [70–72]. It will therefore be interesting to discover the extent to

which a competition between ordering on the intermediate and extended length scales provides a means for rationalizing the density dependent structural transitions that occur in tetrahedral network glass forming systems. Indeed, large scale molecular dynamics simulations based, for example, on the polarizable ion model [73] would be useful in order to give insight into basic issues such as (i) the communality of the principal peak positions in the measured $S_{IJ}(k)$ for network glass forming AX_2 materials and (ii) whether this occurrence is a necessary condition for the formation of a marked FSDP. Furthermore, although the rigid-ion model of equation (9) gives an excellent starting point for describing the properties of many molten salts, it is not clear why equations (10)–(12) appear to remain valid for glass forming AX_2 systems since three- or higher-body interactions are usually required in order to provide a realistic representation of the measured structural and dynamical properties [22, 34]. Molecular dynamics simulations will enable the generality of equations (10)–(12) to be rigorously tested and will hence give additional insight into the nature of extended range oscillations.

5. Conclusions

The experimental results for tetrahedral network glass forming AX_2 systems show that the structure is described by two characteristic length scales at distances greater than the nearest-neighbour. The ordering that extends to the largest distances is *not* the intermediate range order, which is associated with the appearance in the measured diffraction patterns of an FSDP, but is instead a local ordering phenomenon which has a *long* coherence length. The periodicity and extent of this ordering on an extended range are set by the position and width, respectively, of the principal peak in the measured diffraction patterns. Further work is required in order to unravel the interrelation between the ordering on the intermediate and extended length scales and its density dependence.

Acknowledgments

It is a pleasure to thank all those who have contributed to the neutron diffraction work, including Ian Penfold and Jian Liu (UEA), Ingrid Petri and Richard Martin (Bath), Adrian Barnes and Phil Mason (Bristol), Pierre Chieux, Gabriel Cuello, Henry Fischer and Pierre Palleau (ILL), Spencer Howells (ISIS) and Chris Benmore (ANL). David Price (Orléans) is also thanked for a useful discussion and Grant Henderson (Toronto) is thanked for pointing out the work by Konnert and Karle. The support of the EPSRC, Institut Laue-Langevin (ILL) and ISIS is gratefully acknowledged.

References

[1] Konnert J H, Karle J and Ferguson G A 1973 *Science* **179** 177
[2] Karle J and Konnert J H 1976 *Phys. Rev. Lett.* **36** 823
[3] Wright A C and Leadbetter A J 1976 *Phys. Chem. Glasses* **17** 122
[4] Enderby J E, North D M and Egelstaff P A 1966 *Phil. Mag.* **14** 961
[5] Boolchand P (ed) 2000 *Insulating and Semiconducting Glasses* (Singapore: World Scientific)
[6] Salmon P S, Martin R A, Mason P E and Cuello G J 2005 *Nature* **435** 75
[7] Moss S C and Price D L 1985 *Physics of Disordered Materials* ed D Adler, H Fritzsche and S R Ovshinsky (New York: Plenum) p 77
[8] Elliott S R 1991 *Nature* **354** 445
[9] Salmon P S 1994 *Proc. R. Soc. Lond.* A **445** 351
[10] Fritzsche H 2000 *Insulating and Semiconducting Glasses* ed P Boolchand (Singapore: World Scientific) p 653
[11] Faber T E and Ziman J M 1965 *Phil. Mag.* **11** 153
[12] Bhatia A B and Thornton D E 1970 *Phys. Rev.* B **2** 3004
[13] Fischer H E, Cuello G J, Palleau P, Feltin D, Barnes A C, Badyal Y S and Simonson J M 2002 *Appl. Phys.* A **74** S160
[14] Fischer H E, Barnes A C and Salmon P S 2006 *Rep. Prog. Phys.* **69** 233
[15] Edwards F G, Howe R A, Enderby J E and Page D I 1978 *J. Phys. C: Solid State Phys.* **11** 1053

[16] McGreevy R L and Mitchell E W J 1982 *J. Phys. C: Solid State Phys.* **15** 5537
[17] Biggin S and Enderby J E 1981 *J. Phys. C: Solid State Phys.* **14** 3577
[18] Biggin S, Gay M and Enderby J E 1984 *J. Phys. C: Solid State Phys.* **17** 977
[19] Newport R J, Howe R A and Wood N D 1985 *J. Phys. C: Solid State Phys.* **18** 5249
[20] Biggin S and Enderby J E 1981 *J. Phys. C: Solid State Phys.* **14** 3129
[21] Müller U 1993 *Inorganic Structural Chemistry* (Chichester: Wiley)
[22] Salmon P S 1992 *Proc. R. Soc. Lond.* A **437** 591
[23] Tosi M P, Price D L and Saboungi M-L 1993 *Annu. Rev. Phys. Chem.* **44** 173
[24] Penfold I T and Salmon P S 1990 *J. Phys.: Condens. Matter* **2** SA233
[25] Penfold I T and Salmon P S 1991 *Phys. Rev. Lett.* **67** 97
[26] Petri I, Salmon P S and Fischer H E 2000 *Phys. Rev. Lett.* **84** 2413
[27] Salmon P S and Petri I 2003 *J. Phys.: Condens. Matter* **15** S1509
[28] Salmon P S, Barnes A C, Martin R A and Cuello G J 2006 *Phys. Rev. Lett.* **96** 235502
[29] Salmon P S, Barnes A C, Martin R A and Cuello G J 2007 *J. Phys.: Condens. Matter* **19** 415110
[30] Price D L, Moss S C, Reijers R, Saboungi M-L and Susman S 1988 *J. Phys. C: Solid State Phys.* **21** L1069
[31] Durben D J and Wolf G H 1991 *Phys. Rev.* B **43** 2355
[32] Polsky C H, Martinez L M, Leinenweber K, VerHelst M A, Angell C A and Wolf G H 2000 *Phys. Rev.* B **61** 5934
[33] Wang F, Mamedov S, Boolchand P, Goodman B and Chandrasekhar M 2005 *Phys. Rev.* B **71** 174201
[34] Salmon P S 2006 *J. Phys.: Condens. Matter* **18** 11443
[35] Grimley D I, Wright A C and Sinclair R N 1990 *J. Non-Cryst. Solids* **119** 49
[36] Dittmar G and Schäfer H 1976 *Acta Crystallogr.* B **32** 2726
[37] Wright A C, Etherington G, Desa J A E, Sinclair R N, Connell G A N and Mikkelsen J C Jr 1982 *J. Non-Cryst. Solids* **49** 63
[38] Anikeenko A V and Medvedev N N 2007 *Phys. Rev. Lett.* **98** 235504
[39] Salmon P S 2007 *J. Non-Cryst. Solids* **353** 2959
[40] Boolchand P and Phillips J C 1992 *Phys. Rev. Lett.* **68** 252
[41] Penfold I T and Salmon P S 1992 *Phys. Rev. Lett.* **68** 253
[42] Salmon P S 2005 *J. Phys.: Condens. Matter* **17** S3537
[43] Sangster M J L and Dixon M 1976 *Adv. Phys.* **25** 247
[44] Wilson M and Madden P A 1993 *J. Phys.: Condens. Matter* **5** 6833
[45] Hutchinson F, Rowley A J, Walters M K, Wilson M, Madden P A, Wasse J C and Salmon P S 1999 *J. Chem. Phys.* **111** 2028
[46] Pyper N C 1991 *Adv. Solid State Chem.* vol 2, ed C R A Catlow (London: JAI Press) p 223
[47] Kjellander R and Forsberg B 2005 *J. Phys. A: Math. Gen.* **38** 5405
[48] Evans R, Leote de Carvalho R J F, Henderson J R and Hoyle D C 1994 *J. Chem. Phys.* **100** 591
[49] Leote de Carvalho R J F and Evans R 1994 *Mol. Phys.* **83** 619
[50] Lorch E 1969 *J. Phys. C: Solid State Phys.* **2** 229
[51] Levashov V A, Billinge S J L and Thorpe M F 2005 *Phys. Rev.* B **72** 024111
[52] Christie J K, Taraskin S N and Elliott S R 2004 *J. Phys.: Condens. Matter* **16** S5109
[53] Christie J K, Taraskin S N and Elliott S R 2004 *Phys. Rev.* B **70** 134207
[54] Angell C A 1995 *Science* **267** 1924
[55] Stølen S, Grande T and Johnsen H-B 2002 *Phys. Chem. Chem. Phys.* **4** 3396
[56] Sastry S 2001 *Nature* **409** 164
[57] Saika-Voivod I, Poole P H and Sciortino F 2001 *Nature* **412** 514
[58] Saika-Voivod I, Sciortino F and Poole P H 2004 *Phys. Rev.* E **69** 041503
[59] Salmon P S and Liu J 1994 *J. Phys.: Condens. Matter* **6** 1449
[60] Mei Q, Benmore C J, Hart R T, Bychkov E, Salmon P S, Martin C D, Michel F M, Antao S M, Chupas P J, Lee P L, Shastri S D, Parise J B, Leinenweber K, Amin S and Yarger J L 2006 *Phys. Rev.* B **74** 014203
[61] Crichton W A, Mezouar M, Grande T, Stølen S and Grzechnik A 2001 *Nature* **414** 622
[62] Ruska J and Thurn H 1976 *J. Non-Cryst. Solids* **22** 277
[63] Petri I, Salmon P S and Howells W S 1999 *J. Phys.: Condens. Matter* **11** 10219
[64] Neuefeind J and Liss K-D 1996 *Ber. Bunsenges. Phys. Chem.* **100** 1341
[65] Dijkstra M and Evans R 2000 *J. Chem. Phys.* **112** 1449
[66] Grodon C, Dijkstra M, Evans R and Roth R 2004 *J. Chem. Phys.* **121** 7869
[67] Hansen J P and McDonald I R 1986 *Theory of Simple Liquids* 2nd edn (Amsterdam: Elsevier)
[68] Poole P H, Grande T, Angell C A and McMillan P F 1997 *Science* **275** 322
[69] Wilding M C, Wilson M and McMillan P F 2006 *Chem. Soc. Rev.* **35** 964
[70] Franzese G, Malescio G, Skibinsky A, Buldyrev S V and Stanley H E 2001 *Nature* **409** 692
[71] Jagla E A 2001 *Phys. Rev.* E **63** 061501
[72] Gibson H M and Wilding N B 2006 *Phys. Rev.* E **73** 061507
[73] Sharma B K and Wilson M 2006 *Phys. Rev.* B **73** 060201